JOURNAL OF COMPUTATIONAL PHYSICS 108, 327–342 (1993)

The Method of Auxiliary Mapping for the Finite Element Solutions of Elliptic Problems Containing Singularities

T. R. LUCAS AND H. S. OH*

Department of Mathematics, University of North Carolina at Charlotte, Charlotte, North Carolina 28223

Received February 18, 1992; revised January 12, 1993

Babuska and Oh have introduced a new approach called *the method of auxiliary mapping* (MAM), to deal with elliptic boundary value problems with singularities. They showed that for the Laplace equation with corner singularities, in the context of the p-version of the finite element method, MAM yielded an exponential rate of convergence at virtually no extra cost. In this paper those results are extended by showing the exponential convergence of MAM for homogeneous Laplace equations with boundary singularities and Helmholtz equations with both corner and boundary singularities. In addition a convergence result is developed for MAM as applied to the h-p version of the finite element method. To clarify the power of MAM a series of benchmark runs are made for three examples using our implementation, MAPFEM. Comparisons are made with two h-version finite element codes (PLTMG6 and FESOP), both of which use adaptive meshes, the finite difference code ELLPACK, and the recent singular element code ISBFM. The examples include the well-known Motz problem and both homogeneous and nonhomogeneous Helmholtz equations.

1. INTRODUCTION

Recently Babuska and Oh [6] introduced a new approach, called *the method of auxiliary mapping* (MAM), to deal with corner singularities. In this paper we make several extensions of MAM, one of which is to include boundary singularities for a more general set of elliptic partial differential equations. The essence of this method involves locally transforming a region around each singularity to a new domain by use of a conformal mapping such as $\xi = \Psi(z) = z^{\beta}$. Here β is directly determined by the known nature of the singularity in such a way as to locally transform the exact (singular) solution to a smoother or even locally analytic function, which can be easily approximated in the new domain by the conventional use of the p-version of the finite element method. For example, consider a strong singularity about the origin in the upper half plane of the form $r^{1/2}f(r, \theta)$, where f is smooth. Then $\Psi(z) = z^{1/2}$ maps the upper half plane into the first quadrant, and a point (ρ, ϕ) in the first quadrant evaluates as $\rho f(\rho^2, 2\phi)$, a smooth function. Thus, MAM allows for the use of ordinary basis functions in the mapped region to approximate a smooth form of the original singular solution.

To further understand the effect of MAM, let $\Omega = \{(r, \theta): r \leqslant L,\ 0 \leqslant \theta \leqslant \pi/4\}$. Then $\Psi(\Omega) = \{(\rho, \phi): \rho \leqslant \sqrt{L},\ 0 \leqslant \phi \leqslant \pi/8\}$ and through the auxiliary mapping Ψ the standard elemental shape functions $\hat{N}_j$ on $\Psi(\Omega)$ become singular functions N_j on Ω. Furthermore, if we consider the basis functions of p-degree 10 over $\Psi(\Omega)$, the singular functions created over Ω through the mapping Ψ *restricted to the positive x-axis* are generated by $\{1, x^{1/2}, x, x^{3/2}, ..., x^{9/2}, x^5\}$. That is, MAM implicitly creates special singular basis functions which mimic the singularity. However, unlike other singular function approaches, MAM is not required to construct or use singular basis functions in actual computations.

In [6], Babuska and Oh showed that MAM in the context of the p-version of the finite element method yielded an exponential rate of convergence at virtually no extra cost, developed requirements for a general auxiliary mapping, and showed that a typical homogeneous problem with a corner singularity converged at an exponential rate. They also discussed a nonhomogeneous problem with a corner singularity, showed that the convergence was proportional to a power of the degrees of freedom N_p, and considered an application to elliptic problems on unbounded domains. As a part of a further investigation of MAM (for problems with a different structure of singularities such as those in elasticity), they showed in [31] that MAM could successfully improve the worst singularities arising from interface problems by a suitable choice of auxiliary mappings.

This paper is organized as follows. In Section 2, we give a general description of MAM. Here we include a general result on how to compute the bilinear form related to the elliptic equation on mapped regions. In Section 3, MAM is shown to converge exponentially for both Laplace

* This work of this author was supported in part by NSF Grant ASC-9113895.

0021-9991/93 $5.00

and Helmholtz operators with combinations of corner and boundary singularities. The forcing term f, if present, is assumed to be locally zero near the singularities. For full exponential convergence using the Helmholtz operator, certain restrictions on the angle of the corner singularities are imposed, although greatly improved results are obtained in any case. In addition a convergence result is developed for MAM as applied to the h-p version of the finite element method. In Section 4 we clarify the power of MAM with a series of benchmark runs for three examples using our implementation, MAPFEM. Comparisons are made with two h-version finite element codes (PLTMG6 and FESOP), both of which use adaptive meshes, the finite difference code ELLPACK and the recent singular element code ISBFM [29]. The examples include the well-known Motz problem and both homogeneous and nonhomogeneous Helmholtz equations. We use the results of [24, 26] for our benchmark comparisons with the Motz problem, after discovering a correction to the value of one of the published coefficients.

In elliptic boundary value problems, singularities are caused by nonsmooth geometric boundaries (corner singularities), by discontinuities in the coefficients of the partial differential equations (interface singularities), or by changes in the type of boundary conditions such as from Dirichlet to Neumann (boundary singularities). These problems are notable for their difficulty [5, 7, 13, 18, 24–26, 29, 31, 35, 37–40]). It is well known that the standard finite element and finite difference methods have problems in providing accurate numerical solutions at a reasonable cost for elliptic boundary value problems containing singularities. Many different approaches have been attempted over the years to provide accurate and economical solutions. The two principal approaches of the past have been mesh refinement [2, 5, 7, 9, 19, 20] and the use of special singular basis functions [1, 13, 21, 22, 24–26, 29, 33–35]. Our results, both theoretical and in practice, show that MAM combines the best features of both of these approaches, providing the accuracy of singular elements but with the convenience and economy of a nonadaptive mesh. Moreover, MAM is an essentially local method, using a separate mapping for each singular region.

2. NOTATION AND BASIC RESULTS

2.1. *Results for General Elliptic Equations of Second Order*

Throughout this paper, Ω and Ω^* will denote simply connected bounded domains of the usual Euclidean space R^2. $\Gamma = \partial\Omega$ denotes the boundary of Ω and $\partial\Omega = \bigcup_{j=1}^{M} \bar{\Gamma}_j$, Γ_j are open line segments called edges. Let $\Psi: \Omega \to \Omega^*$ be a bijective mapping. We will denote the Jacobian of Ψ by $J(\Psi)$, and its determinant by $|J(\Psi)|$. Although we focus on the Laplace and Helmholtz operators in this paper, the mapping technique can be extended to general elliptic operators. Thus, we start with the following elliptic boundary value problem:

$$-\mathscr{L}(u) + a_0 u = f \qquad \text{in } \Omega, \tag{1}$$

$$u = 0 \qquad \text{on } \Gamma_D, \tag{2}$$

$$\frac{\partial u}{\partial n_c} = h \qquad \text{on } \Gamma_N, \tag{3}$$

where $\mathscr{L} = \sum (\partial/\partial x_j)(a_{ij}(x)(\partial/\partial x_i))$ is strongly elliptic, $\partial u/\partial n_c = \sum a_{ij}(x)\, v_j(\partial u/\partial x_i)$ is the conormal derivative, $\Gamma_D \cup \Gamma_N = \partial\Omega$, $a_0 \geq 0$, $a_0(x) \in L_\infty(\Omega)$, $a_{ij}(x) \in L_\infty(\Omega)$, $f \in L^2(\Omega)$, $h \in L^2(\Gamma_N)$.

Let $H^1(\Omega)$ be the usual Sobolev space and $H^1_D(\Omega) = \{u \in H^1(\Omega) : u = 0 \text{ on } \Gamma_D\}$. For $u, v \in H^1(\Omega)$, we let

$$B(u, v) = \int_\Omega \left\{ \sum a_{ij} \frac{\partial u}{\partial x_i} \frac{\partial v}{\partial x_j} + a_0 uv \right\} dx$$

$$F(v) = \int_\Omega fv\, dx + \int_{\Gamma_N} hv\, d\gamma.$$

By the exact solution of (1)–(3), we mean $u_{ex} \in H^1_D(\Omega)$ such that

$$B(u, v) = F(v) \qquad \text{for all} \quad v \in H^1_D(\Omega). \tag{4}$$

Let us denote $B(u, u)$ by $\|u\|_E^2$ and the energy norm by $\|\cdot\|_E$. It was shown in [12] that if the measure $(\Gamma_D) > 0$ then $\|\cdot\|_E$ is equivalent to $\|\cdot\|_{H^1(\Omega)}$ on $H^1_D(\Omega)$.

Consider a bijective mapping $\Psi: \Omega \to \Omega^*$ and for any $u: \Omega \to R$, the related function $\hat{u} = u \circ \Psi^{-1}: \Omega^* \to R$. More generally we denote $J(\Psi) \circ \Psi^{-1}$ by $\widehat{J(\Psi)}$. The following theorem shows how to compute the bilinear form related to an elliptic operator over the mapped functions $\hat{u}$ and $\hat{v}$ in Ω^*. This result is useful not only for the results of this paper but also in the applications of MAM to more complicated singularity structures such as three-dimensional problems [30] or interface singularities.

THEOREM 2.1. *Let $\Psi: \Omega \to \Omega^*$ be a bijective mapping. Suppose q_{kl} denotes the (k, l)-component of the symmetric matrix,*

$$Q = |J(\Psi^{-1})|\, \widehat{J(\Psi)} \cdot [\hat{a}_{ij}(\xi)] \cdot \widehat{J(\Psi)}^{\mathrm{T}}, \tag{5}$$

where $a_{ij}(x) \in L_\infty(\Omega)$ for all i and j. Then for any u, v in $H^1(\Omega)$ and corresponding functions $\hat{u} = u \circ \Psi^{-1}$, $\hat{v} = v \circ \Psi^{-1}$,

$$\int_\Omega \sum a_{ij}(x) \frac{\partial u}{\partial x_i} \frac{\partial v}{\partial x_j} = \int_{\Omega^*} \sum q_{kl}(\xi) \frac{\partial \hat{u}}{\partial \xi_k} \frac{\partial \hat{v}}{\partial \xi_l},$$

where $q_{kl}(\xi) \in L_\infty(\Omega^*)$.

Proof.

$$\int_\Omega \sum a_{ij}(x)\frac{\partial u}{\partial x_i}\frac{\partial v}{\partial x_j}$$

$$= \int_\Omega \nabla u \cdot [a_{ij}(x)] \cdot \nabla v^{\mathrm{T}}$$

$$= \int_\Omega \nabla \hat{u} \cdot J(\Psi) \cdot [a_{ij}(x)] \cdot J(\Psi)^{\mathrm{T}} \cdot \nabla \hat{v}^{\mathrm{T}}$$

$$= \int_{\Omega^*} |J(\Psi^{-1})| \, \nabla \hat{u} \cdot \widehat{J(\Psi)} \cdot [\hat{a}_{ij}(\xi)] \cdot \widehat{J(\Psi)}^{\mathrm{T}} \cdot \nabla \hat{v}^{\mathrm{T}}$$

$$= \int_{\Omega^*} \sum q_{kl}(\xi)\frac{\partial \hat{u}}{\partial \xi_k}\frac{\partial \hat{v}}{\partial \xi_l}. \qquad \text{Q.E.D.}$$

COROLLARY 2.1. *Suppose Ω and Ω^* are domains in R^2. If Ψ is a conformal mapping, then we have*

$$\int_\Omega \nabla u \cdot \nabla v \, dx = \int_{\Omega^*} \nabla \hat{u} \cdot \nabla \hat{v} \, d\xi. \tag{6}$$

Proof. Since Ψ is conformal, the coordinate functions of Ψ satisfy the Cauchy–Riemann equations. Hence, a direct calculation shows that $J(\Psi) \cdot J(\Psi)^{\mathrm{T}} = |J(\Psi)| \cdot I$, where I denotes the identity matrix. Hence by Theorem 2.1, $Q = |J(\Psi^{-1})| \, \hat{J}(\Psi) \cdot I \cdot \hat{J}(\Psi)^{\mathrm{T}} = I$ giving the result. Q.E.D.

2.2. *The Method of Auxiliary Mapping*

From now on, we will consider the two-dimensional model problem

$$-\Delta u + a_0 u = f \qquad \text{on } \Omega \tag{7}$$

$$u = 0 \qquad \text{on } \Gamma_D = \bigcup_{i \in \mathscr{D}} \bar{\Gamma}_i \tag{8}$$

$$\frac{\partial u}{\partial n} = h \qquad \text{on } \Gamma_N = \bigcup_{i \in \mathscr{N}} \bar{\Gamma}_i, \tag{9}$$

where a_0 is a nonnegative real number, $\Omega \subset R^2$ is a bounded polygonal domain whose boundary Γ is composed of open straight line segments Γ_i with $\bigcup \bar{\Gamma}_i = \Gamma$, $\mathscr{D}$ and $\mathscr{N}$ are disjoint, $f \in L^2(\Omega)$, and $h \in L^2(\Gamma_N)$. If $a_0 = 0$, the left-hand side of (7) is the Laplace operator while if $a_0 > 0$ it is the Helmholtz operator.

Suppose that the exact solution u_{ex} of (7)–(9) has a boundary singularity (caused by a change from a Dirichlet to a Neumann boundary condition, as shown in Example A of Section 4) or corner singularity at the vertices A_q, $q = 1, \ldots, s$.

Throughout this paper, $\pi\omega_q$ denotes the internal angle of the vertex of a singular point A_q (see Fig. 2.1) and $\Omega_q = \{z : |z - A_q| \leqslant r_q\} \cap \Omega$ denotes a singular neighborhood of A_q of the form of a circular sector in Ω. It will be assumed that $h = 0$ along $\Gamma_N \cap \Omega_q$ and $f = 0$ on Ω_q for all q corresponding to singular points A_q.

Now, for any positive α we would like to introduce a conformal mapping $\Psi_q : \Omega_q \to \Omega_q^*$ which will play an essential role throughout this paper:

$$\Psi_q^{-1} \equiv \varphi^\alpha : z = \xi^\alpha, \qquad \text{where } z = x_1 + ix_2 \in \Omega_q, \quad \xi = \xi_1 + i\xi_2 \in \Omega_q^*. \tag{10}$$

The determinants of the Jacobian of φ^α and its inverse Ψ_q are

$$\alpha^2 \rho^{2(\alpha-1)}, \qquad \frac{1}{\alpha^2} r^{2(1-\alpha)/\alpha},$$

respectively. Here (r, θ) denotes polar coordinates in Ω_q and (ρ, ϕ) denotes polar coordinates in $\Omega_q^* = \Psi_q(\Omega_q)$.

Now it can be easily shown that the form of the exact solution u_{ex} on Ω_q for sufficiently small r is of the form of either

$$u_{\mathrm{ex}} = \sum_{k=1}^{\infty} b_k r^{k/\omega_q} \sin(k\theta/\omega_q) \tag{11}$$

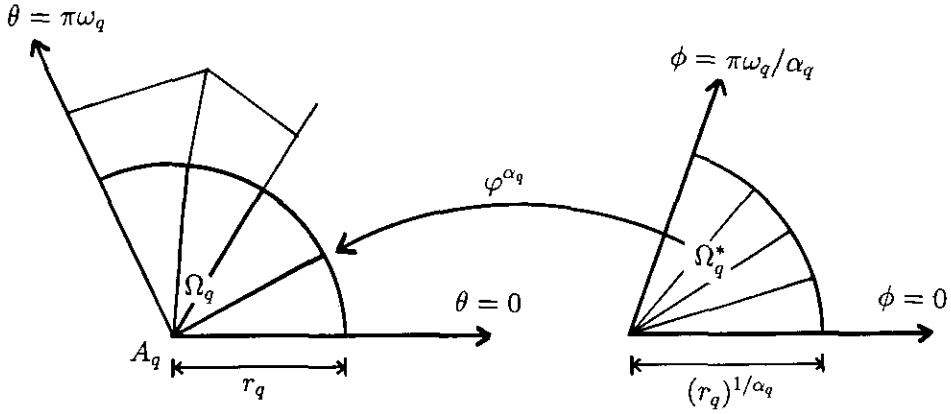

FIG. 2.1. A singular neighborhood Ω_q of a singular point A_q and its mapped domain Ω_q^* under the mapping φ^{α_q}. The scheme of mesh $\mathscr{T}_q^*$ on Ω_q^* and the corresponding mesh $\mathscr{T}_q$ on Ω_q.

or

$$u_{ex} = \sum_{k=0}^{\infty} b_k r^{(k+1/2)/\omega_q} \cos((k+1/2)\,\theta/\omega_q) \qquad (12)$$

in the case of $a_0 = 0$ (Laplace operator), according as A_q is a corner singularity or a boundary singularity. If $a_0 > 0$ (Helmholtz operator), the respective equations are

$$u_{ex} = \sum_{k=1}^{\infty} b_k I_{k/\omega_q}(a_0 r) \sin(k\theta/\omega_q) \qquad (13)$$

or

$$u_{ex} = \sum_{k=0}^{\infty} b_k I_{(k+1/2)/\omega_q}(a_0 r) \cos((k+1/2)\,\theta/w_q), \qquad (14)$$

where

$$I_\lambda(a_0 r) = \left(\frac{a_0 r}{2}\right)^{\lambda} \sum_{l=0}^{\infty} \frac{a_0^{2l} r^{2l}}{4^l l!\, \Gamma(l+1+\lambda)}$$

is the modified Bessel function of the first kind of order λ.

We now describe the *method of auxiliary mapping*:

Step 1. *Selection of singular regions.* For each singularity A_q choose a singular neighborhood of the form of a circular sector:

$$\Omega_q = \{z : |z - A_q| \leqslant r_q\} \cap \Omega.$$

The size of the radius r_q is restricted so that h is zero along $\Gamma \cap \partial\Omega_q$ and f is zero on Ω_q. If possible, it is desirable to choose a larger radius to avoid the pollution effect on $\Omega \backslash \Omega_q$, caused by the singularity at A_q, but not so large that $\hat{u} = u \circ \Psi_q^{-1}$ fails to be analytic on Ω_q^*.

Step 2. *Construction of auxiliary mappings.* Let Ψ_q: $\Omega_q \to \Omega_q^*$ be a conformal mapping defined by an integer m_q and the number ω_q:

$$\Psi_q^{-1} \equiv \varphi^{m_q \omega_q} : z = \xi^{m_q \omega_q}. \qquad (15)$$

The integer m_q must satisfy two requirements: $m_q \omega_q > 1$ (required by Lemma 3.1) and if A_q is a boundary singularity, m_q is even, i.e., of the form $m_q = 2n_q$. Let us recall that $\pi\omega_q$ is the interior angle at A_q. Then the auxiliary mapping defined by (15) transforms u_{ex} on Ω_q of the forms (11)–(14) into $\hat{u}_{ex} = u_{ex} \circ \Psi_q^{-1}$ on Ω_q^* of the forms

$$\hat{u}_{ex} = \sum_{k=0}^{\infty} b_k \rho^{km_q} \sin(m_q k\phi), \qquad (16)$$

$$\hat{u}_{ex} = \sum_{k=0}^{\infty} b_k \rho^{(2k+1)n_q} \cos(n_q(2k+1)\phi), \qquad (17)$$

$$\hat{u}_{ex} = \sum_{k=1}^{\infty} b_k \left(\frac{a_0}{2}\right)^{k/\omega_q} \rho^{km_q} \times \left[\sum_{l=0}^{\infty} \frac{a_0^{2l} \rho^{2lm_q\omega_q}}{4^l l!\, \Gamma(l+1+k/\omega_q)}\right] \sin(m_q k\phi), \qquad (18)$$

$$\hat{u}_{ex} = \sum_{k=0}^{\infty} b_k \left(\frac{a_0}{2}\right)^{(k+1/2)/\omega_q} \rho^{(2k+1)n_q} \times \left[\sum_{l=0}^{\infty} \frac{a_0^{2l} \rho^{4ln_q\omega_q}}{4^l l!\, \Gamma(l+1+(k+1/2)/\omega_q)}\right] \times \cos(n_q(2k+1)\phi), \qquad (19)$$

respectively. Let us note that for sufficiently small ρ, $\hat{u}_{ex}$ in (16) and (17) is analytic; $\hat{u}_{ex}$ in (18) and (19) is also analytic for a suitable choice of m_q, provided that ω_q is a rational number. If ω_q is an irrational number, $\hat{u}_{ex}$ in (18) and (19) cannot be analytic, but will be highly regular. In practice, we will choose m_q in (16) and (18) and n_q in (17) and (19) to be the smallest integer such that $m_q\omega_q > 1$. It was shown in [6] that MAM with $m_q \gg 1$ yields highly improved results when basis functions are of higher order. The success of an application of MAM depends critically on finding mappings Ψ_q, such that $\hat{u}_{ex}$ is smoother.

Step 3. *Construction of mesh.* Subdivide Ω into triangles and rectangles so that, for each singular neighborhood Ω_q, $\partial\Omega_q$ consists of sides of elements. Let us note that curves are allowed for interior sides in a mesh for the p-version of the finite element method (see Fig. 2.1 or Mesh I in Fig. 4.1). More precisely, for each Ω_q, generate a triangulation $\mathcal{T}_q^*$ of Ω_q^* and generate a triangulation $\mathcal{T}_q$ on Ω_q as the image of $\mathcal{T}_q^*$ under Ψ_q^{-1}. Then construct a triangulation $\mathcal{T}$ on Ω so that $\mathcal{T}|_{\Omega_q} = \mathcal{T}_q$ for each q. Let $\Omega_0 = \Omega \backslash [\bigcup_{q=1}^{s} \Omega_q]$ and $\mathcal{T}|_{\Omega_0} = \mathcal{T}_0$ be a triangulation of the remaining (nonsingular) region.

In the next step, we describe the special singular functions generated through Ψ_q^{-1} which mimic the original singularities. We also explain how to directly compute elemental stiffness matrices and elemental load vectors without *constructing* any special singular functions:

Step 4. *Computation of local stiffness matrices and local load vectors on the elements in singular regions:*

(a) Let e be an element in a singular neighborhood Ω_q and $e^* = \Omega_q(e)$ be the corresponding (curvilinear) element in Ω_q^*. Let Φ_{e^*} be the usual elemental mapping function (since we allow curved sides, it is of the *blending* type as used in [36]) from a standard element E (see Section 3 for details) onto the element e^*. These mappings then induce the *singular elemental map* Φ_e^S from E onto the original element e defined by $\Phi_e^S = \Psi_q^{-1} \circ \Phi_{e^*}$.

(b) For the computation of the stiffness matrices and the load vectors on elements e, apply the following rule:

(1) Use the singular elemental mappings, Φ_e^S, if $e \subset [\bigcup_{q=1}^s \Omega_q]$

(2) Use the standard elemental mappings, Φ_e, if $e \subset \Omega_0$.

From Corollary 2.1, for $e \subset \bigcup_{q=1}^s \Omega_q$, we have

$$\int_e \{\nabla N_i \cdot \nabla N_j + a_0 N_i N_j\} = \int_{e^*} \{\nabla N_i^* \cdot \nabla N_j^* + a_0 |J(\Psi_q^{-1})| N_i^* N_j^*\}, \quad (20)$$

where $N_i = N_i^* \circ \Psi_q$, $N_i^* = \mathcal{N}_i \circ \Phi_{e^*}^{-1}$, and $\mathcal{N}_i$ is a standard shape function on the standard element E. Thus, using the singular elemental mapping in rule (1) of Step 4 is the same as using the right-hand sides of (20). It is worth noting that the shape functions, $N_i = \mathcal{N}_i \circ (\Phi_e^S)^{-1} = \mathcal{N}_i \circ \Phi_{e^*}^{-1} \circ \Psi_q$, are singular functions which mimic the singularity. N_i^* and N_j^* are conventional shape functions constructed through the conventional elemental mapping Φ_{e^*} and hence no special quadrature coding is needed for the right-hand sides of (20). They can be computed by any existing code. Actually we neither construct any special functions for elemental stiffness matrices and elemental load vectors on $e \subset \Omega_q$ nor will we require these special functions in postprocessing.

Let us note that if $\Psi_q^{-1} = \varphi^\alpha$ is the conformal mapping defined by (10), for the singular elemental mappings Φ_e^S, $|J(\Phi_e^S)|$ is not bounded away from zero (i.e., it does not satisfy (21a) below). Nevertheless from Corollary 2.1, $|J(\varphi^\alpha)|$ is canceled out in the computation of the stiffness matrices.

We require that these elemental mapping satisfy the usual conditions used in the finite element method that lead to *conforming finite elements*. That is, we will require that each elemental mapping Φ_e on $e \subset [\Omega \backslash \bigcup_{q=1}^s \Omega_q]$ (Φ_{e^*} on $e^* \subset [\bigcup_{q=1}^s \Omega_q^*]$) satisfies the following technical conditions [2, 20] so that they lead to conforming elements. Let h be the maximum length of the sides of the curvilinear element e^h. Then the bijective mapping $\Phi_e(s, t) = (x_1(s, t), x_2(s, t)) : E \to e^h$ satisfies

$$C_1 h^2 \leqslant |J(\Phi_e)| \leqslant C_2 h^2. \quad (21a)$$

$$|D^\beta x_1| \leqslant Ch^{|\beta|}, \ |D^\beta x_2| \leqslant Ch^{|\beta|}, \ |\beta| \leqslant k,$$
where k is to be a positive integer
and β is a multi-index. (21b)

$$\text{Let } \Phi_e^{-1}(x_1, x_2) = (s(x_1, x_2), t(x_1, x_2)), \text{ then}$$
$$|D^\beta s| \leqslant Ch^{-1}, \ |D^\beta t| \leqslant Ch^{-1} \text{ for } |\beta| = 1. \quad (21c)$$

If A_l and γ_l denote the vertices and sides of e^h,
then $\Phi_e^{-1}(A_l)$ and $\Phi_e^{-1}(\gamma_l)$ are vertices and sides of E.
Moreover, if $\Phi_{e_i} : E \to e_i$ and $\Phi_{e_j} : E \to e_j$
and $\bar{e}_i \cap \bar{e}_j = \gamma$, where γ has endpoints A_1 and A_2,
then for any $B \in \gamma$, $\operatorname{dist}(\Phi_{e_j}^{-1}(B), \Phi_{e_j}^{-1}(A_l))$
$= \operatorname{dist}(\Phi_{e_i}^{-1}(B), \Phi_{e_i}^{-1}(A_l)), \ l = 1, 2.$ (21d)

It is important to note that the auxiliary mappings defined by (15) are linear on the arc length. Thus, the elements constructed from these standard elemental shape function Φ_e and singular elemental shape functions Φ_e^S are *conforming*.

3. CONVERGENCE RATES

The set of all algebraic polynomials of (total) degree less than or equal to p on E will be denoted by $\mathcal{P}_p^1(E)$. By $\mathcal{P}_p^2(E)$ we will denote the set of all polynomials of degree less than or equal to p in each variable on E. By $\mathcal{P}_p(E)$ we mean $\mathcal{P}_p^1(E)$ if $E = T$ and $\mathcal{P}_p^2(E)$ if $E = Q$, respectively. Here $T = \{(\xi, \eta) : |\xi| \leqslant 1 - \eta/\sqrt{3}, \ 0 \leqslant \eta \leqslant \sqrt{3}\}$ and $Q = \{(\xi, \eta) : -1 \leqslant \xi \leqslant 1, \ -1 \leqslant \eta \leqslant 1\}$ are the reference triangle and rectangle, respectively.

LEMMA 3.1. *Let* $\Omega_q = \{z : |z - A_q| < R_q\} \cap \Omega$ *and* $e \in \mathcal{T}_q$. *Suppose* Ψ_q^{-1} *is given by* (10) *with* $\alpha > 1$ *and* $v \in H^1(\Omega)$. *Let* $\hat{v} = v \circ \Psi_q^{-1}$. *Then* $\|v\|_{1,e} \leqslant \sqrt{\max(1, \alpha^2 R_q^{2(\alpha-1)/\alpha})}\, \|\hat{v}\|_{1,e^*}$.

Proof. $\int_e |v|^2 \, dx = \int_{e^*} |J(\varphi^\alpha)| \, |v \circ \varphi^\alpha|^2 \, d\xi = \int_{e^*} \alpha^2 \rho^{2(\alpha-1)} |\hat{v}|^2 \, d\xi \leqslant \alpha^2 R_q^{2(\alpha-1)/\alpha} \|\hat{v}\|_{0,e^*}^2$. On the other hand, by Corollary 2.1, $|v|_{1,e}^2 = |\hat{v}|_{1,e^*}^2$, which completes the proof. Q.E.D.

Let $S_p = \{u \in H_D^1(\Omega) : u|_e \circ \Phi_e \in \mathcal{P}_p(E)$ for all elements $e \in \mathcal{T}\}$, where E is T or Q according as e is a triangular or rectangular element. Then the *p-version of the finite element method* is as follows: find an element $u_p \in S_p$ such that

$$B(u_p, v) = F(v) \qquad \text{for all} \quad v \in S_p.$$

The dimension of S_p will be denoted by N_p and will be called the *degrees of freedom*. In the p-version of the finite element method the triangulation is fixed and only the degree p of the basis polynomials is increased. If $u_{\text{ex}} \in H_D^1(\Omega)$ is the solution then

$$\|u_p - u_{\text{ex}}\|_E = \min_{w \in S_p} \|w - u_{\text{ex}}\|_E.$$

When MAM is used in the framework of the p-version, the finite dimensional space S_p consists of $u \in H_D^1(\Omega)$ such that

$$u|_e \circ \Phi_e \in \mathcal{P}_p(E) \qquad \text{for all} \quad e \subset \Omega_0,$$

$$u|_e \circ \Phi_e^S \in \mathcal{P}_p(E) \qquad \text{for all} \quad e \subset \left[\bigcup_{q=1}^s \Omega_q\right].$$

THEOREM 3.1. *Consider problem* (7)–(9). *Assume all singularities are due to a finite set of s corner or boundary singular points A_q with singular neighborhoods Ω_q, where $f=0$ on Ω_q, and $h=0$ on $\Gamma_N \cap \Omega_q$, $1 \leqslant q \leqslant s$. Assume that in the region Ω_0 away from the singularity, u_{ex} satisfies,*

$$\|u_{ex}\|_{k,\Omega_0} \leqslant CD^k k!, \quad k = 1, 2, \ldots, \text{ for some fixed constants } C \text{ and } D. \tag{22}$$

Let $u_p^{\alpha_1,\ldots,\alpha_s}$ be the finite element solution obtained by employing MAM with the auxiliary mappings $\Psi_q^{-1}: z = \xi^{\pi/\alpha_q}$, $\alpha_q = m_q \omega_q$, defined by (15) *in the framework of the p-version of the finite element method (if $a_0 > 0$ we also require that ω_q be rational and that m_q be chosen so that $2lm_q\omega_q$ is an integer). Then*

$$\|u_p^{\alpha_1,\ldots,\alpha_s} - u_{ex}\|_{H^1(\Omega)} \leqslant C \exp(-\beta \sqrt{N_p}), \tag{23}$$

where C and β are independent of p.

Proof. The proof of this theorem depends essentially on the expansions (11)–(14) and (16)–(19) but otherwise is similar to [6], and is omitted for brevity. Let us note that if u_{ex} is analytic on Ω_0 then it satisfies (22). Q.E.D.

In Section 2 MAM is described for the case when $f = 0$ in the singular neighborhoods. But our method also applies in the case when $f \neq 0$. In such a case, auxiliary mappings may not transform the exact solution u_{ex} of (7)–(9) to an analytic function (see [6]), but can still enhance the rate of convergence.

For example, consider a Poisson equation $-\Delta u = f$ on the L-shaped domain with a corner angle of $\omega_q \pi = 3\pi/2$ at the origin $(0, 0)$ and homogeneous Dirichlet boundary conditions. If $f \in H^0(\Omega)$, then the solution u_{ex} in $\Omega_q = \{(r, \theta): 0 \leqslant \theta \leqslant 3\pi/2, \quad r \leqslant r_q\}$ can be written in the form ([17])

$$u_{ex}(r, \theta) = \sum_{k=0}^{n} a_k r^{(2k/3)} \sin(2k\theta/3) + \sum_{k=1}^{n/3} b_k r^{2k} \log r \sin 2k\theta + v(r, \theta), \tag{24}$$

where $v \in H^2(\Omega_q)$, provided that $\frac{2}{3}(n+1) > 1$. Then $u_{ex} \in H^{k_q}(\Omega_q)$, where $k_q = \frac{5}{3} - \varepsilon$ for an arbitrary positive number ε. That is, $k_q < 2$. On the other hand, if we choose the auxiliary mapping defined by $\Psi_q^{-1}(\xi) = \xi^{3/2}$, $\hat{u}_{ex}$, on $\Omega_q^* = \{(\rho, \phi): 0 \leqslant \phi \leqslant \pi, \rho \leqslant r_q^{2/3}\}$, satisfies

$$\Delta_\xi \hat{u}_{ex}(\xi, \eta) = ((\Delta_x u_{ex}) \circ \Psi_q^{-1}) \left| \frac{d}{d\xi} \Psi_q^{-1}(\xi) \right|^2 = (-f \circ \Psi_q^{-1})(\alpha^2 \rho^{2(\alpha-1)}),$$

where $\alpha = \frac{3}{2}$. Thus, the shift theorem implies $\hat{u}_{ex}$ is at least in $H^2(\Omega_q^*)$. See Example C of Section 4 for an example, where MAM is applied to a nonhomogeneous Helmholtz equation, giving excellent results.

In the remainder of this section we will extend MAM to the *h-p* version of the finite element method. These results can be applied to the above situations in which $\hat{u}_{ex}$ is smoother than u_{ex} but not highly smooth. The following lemma was proven in [9].

LEMMA 3.2. *Let $E = T$ or Q be the reference triangle or rectangle. Suppose $u \in H^k(E)$. Then there exists a family of operators $\{\bar{\pi}_p: H^k(E) \to \mathcal{P}_p(E), p = 1, 2, \ldots\}$ such that for any $0 \leqslant t \leqslant k$,*

$$\|u - \bar{\pi}_p(u)\|_t \leqslant Cp^{-(k-t)} \|u\|_{k,E} \tag{25}$$

$$|(u - \bar{\pi}_p(u))(x)| \leqslant Cp^{-(k-1)} \|u\|_{k,E} \quad \text{if} \quad k > 3/2, \quad x \in E, \tag{26}$$

where the constants C in (25) *and* (26) *are independent of u and p but depend on k. If $u \in \mathcal{P}_p(E)$, then $\bar{\pi}_p(u) = u$.*

Let $\mathcal{T} = \{\mathcal{T}^h\}$, $h > 0$, be a family of meshes $\mathcal{T}^h = \mathcal{T}_0^h \cup [\bigcup_{q=1}^s \mathcal{T}_q^h]$, such as those defined in Step 3 of Section 2. Suppose e^h is either a curvilinear triangular or rectangular element. Let h_{e^h} denote the maximum side length of

$$e^h \quad \text{if} \quad e^h \in \mathcal{T}_0^h \equiv \mathcal{T}^h \Big\backslash \bigcup_{q=1}^{s} \mathcal{T}_q^h;$$

$$(e^h)^* \quad \text{if} \quad e^h \in \bigcup_{q=1}^{s} \mathcal{T}_q^{h/}.$$

Let $\delta_{e^h} = \sup\{\text{diam}(B): B \text{ is a disk in } e^h((e^h)^* \text{ if } e^h \subset [\bigcup_{q=1}^s \Omega_q])\}$. We shall assume that the family $\mathcal{T}$ is *regular* in the sense that there exist positive constants σ, τ independent of $\mathcal{T}^h$ such that for any $\mathcal{T}^h \in \mathcal{T}$, if we define $h = \max_{e^h \in \mathcal{T}^h} h_{e^h}$ then for all $e^h \in \mathcal{T}^h$,

$$\frac{h}{h_{e^h}} \leqslant \tau, \qquad \frac{h_{e^h}}{\delta_{e^h}} \leqslant \sigma.$$

Let

$$S_p^h(\Omega) = \Big\{ u \in H_D^1(\Omega): u|_{e^h} \circ \Phi_{e^h} \in \mathcal{P}_p(E) \text{ for all } e^h \in \mathcal{T}_0^h, \quad u|_{e^h} \circ \Phi_{e^h}^S \in \mathcal{P}_p(E) \text{ for all } e^h \in \bigcup \mathcal{T}_q^h \Big\},$$

where E is Q or T according as e^h is a curvilinear rectangular element or triangular element. Then the *h-p version*

of the finite element method with MAM consists (for a given p and h) of finding $u_p^h \in S_p^h(\Omega)$ such that $B(u_p^h, v) = F(v)$, for all $v \in S_p^h(\Omega)$.

Let

$$\mathscr{Q}_p(e^h) = \{v \circ \Phi_{e^h}^{-1} : v \in \mathscr{P}_p(E)\}, \qquad \text{if} \quad e^h \subset \Omega_0$$

$$\mathscr{Q}_p(e^h) = \{v \circ (\Phi_{e^h}^S)^{-1} : v \in \mathscr{P}_p(E)\}, \qquad \text{if} \quad e^h \subset \left[\bigcup_{q=1}^{s} \Omega_q\right].$$

Let us recall that $(\Phi_{e^h}^S) = \Psi_q^{-1} \circ \Phi_{(e^h)^*}$ if all $e^h \subset \Omega_q$ and that $\Phi_{e^h} : E \to e^h$ and $\Phi_{(e^h)^*} : E \to (e^h)^*$ satisfy condition (24).

Let us define an operator π_p^h from $H^k(e^h)$ onto $\mathscr{Q}_p(e^h)$ by

$$\pi_p^h(u) = \bar{\pi}_p(u \circ \Phi_{e^h}) \circ \Phi_{e^h}^{-1} \qquad \text{for} \quad u \in H^k(e^h), \text{ if } e^h \subset \Omega_0$$

$$\pi_p^h(u) = \bar{\pi}_p(u \circ \Phi_{e^h}) \circ (\Phi_{e^h}^S)^{-1}$$

$$\text{for} \quad u \in H^k(e^h), \text{ if } e^h \subset \left[\bigcup_{q=1}^{s} \Omega_q\right].$$

LEMMA 3.3. *Let $\mathscr{T}^h \in \tilde{\mathscr{T}}$. Suppose for all $e^h \in \mathscr{T}_0^h$, $u \in H^{k_0}(e^h)$, and for all $e^h \in \mathscr{T}_q^h$, $\hat{u} = u \circ \Psi_q^{-1} \in H^{k_q^*}((e^h)^*)$, where k_0 and k_q^* are $\geqslant 1$. Then we have*

$$\|u - \pi_p^h(u)\|_{1, e^h} \leqslant C \frac{h^{\mu_0 - 1}}{p^{k-1}} \|u\|_{k_0, e^h} \qquad \text{if} \quad e^h \in \mathscr{T}_0^h \tag{27}$$

$$\|u - \pi_p^h(u)\|_{1, e^h} \leqslant C \frac{h^{\mu_q - 1}}{p^{k-1}} \|\hat{u}\|_{k_q^*, (e^h)^*} \qquad \text{if} \quad e^h \in \mathscr{T}_q^h \tag{28}$$

$$|(u - \pi_p^h(u))(x)| \leqslant C \frac{h^{\mu_0 - 1}}{p^{k-1}} \|u\|_{k_0, e^h} \qquad \text{if} \quad k > \tfrac{3}{2}, \quad x \in e^h \in \mathscr{T}_0^h, \tag{29}$$

$$|(u - \pi_p^h(u))(x)| \leqslant C \frac{h^{\mu_q - 1}}{p^{k-1}} \|\hat{u}\|_{k_q^*, (e^h)^*} \qquad \text{if} \quad k > \tfrac{3}{2}, \quad x \in e^h \in \mathscr{T}_q^h, \tag{30}$$

where $\mu_0 = \min(k_0, p+1)$ if $e^h \in \mathscr{T}_0^h$, $\mu_q = \min(k_q^*, p+1)$ if $e^h \in \mathscr{T}_q^h$. If μ_0 (μ_q) $> \frac{3}{2}$ and $e^h \in \mathscr{T}_0^h$ ($\mathscr{T}_q^h$), then we can assume that $\pi_p^h(u) = u$ at all vertices of e^h.

Proof. As the proof is similar to that given in [9], we only outline the main steps. For notational simplicity let $(k, \mu) = (k_0, \mu_0)$ or (k_q^*, μ_q), according as $e_h \in \mathscr{T}_0^h$ or $\mathscr{T}_q^h$. Let us consider the case when $\mu = p+1$ (i.e., $k \geqslant p+1$) and k is an integer:

(i) By (21) if $e^h \in \mathscr{T}_0^h$ (and by Lemma 3.1 and (21) if $e^h \in \mathscr{T}_q^h$):

$$\|u - \pi_p^h(u)\|_{1, e^h} \leqslant C \|\bar{u} - \bar{\pi}_p^h(\bar{u})\|_{1, E}.$$

(ii) From the assumptions on Φ_{e^h}, $\bar{u} = u \circ \Phi_{e^h} \in H^k(E)$. By (25) with $t = 1$,

$$\|\bar{u} - \bar{\pi}_p(\bar{u})\|_{1, E} = \|(\bar{u} - z) - \bar{\pi}_p(\bar{u} - z)\|_{1, E} \tag{31}$$

$$\leqslant C p^{-(k-1)} \|\bar{u} - z\|_{k, E}$$

$$\text{for} \quad z \in \mathscr{P}_p(E). \tag{32}$$

(iii) $\|\bar{u} - z\|_{k, E} \leqslant \|\bar{u} - z\|_{\mu, E} + \sum_{j=\mu+1}^{k} |\bar{u}|_{j, E}$ for all $z \in \mathscr{P}_p(E)$.

(iv) By Theorem 3.1.1 of [12],

$$\inf_{z \in \mathscr{P}_p(E)} \|\bar{u} - z\|_{\mu, E} \leqslant C |\bar{u}|_{\mu, E}.$$

(v) By the assumptions on Φ_{e^h} ($\Phi_{(e^h)^*}$ for $e^h \in \mathscr{T}_q^h$) in (21), we have for $\mu \leqslant j \leqslant k$ that

$$|\bar{u}|_{j, E} \leqslant C h^{j-1} \|u\|_{j, e^h} \qquad \text{if} \quad e^h \in \mathscr{T}_0^h, \tag{33}$$

$$|\bar{u}|_{j, E} \leqslant C h^{j-1} \|\hat{u}\|_{j, (e^h)^*} \qquad \text{if} \quad e^h \in \mathscr{T}_q^h. \tag{34}$$

(vi) Therefore by (i)–(v),

$$\|u - \pi_p^h(u)\|_{1, e^h} \leqslant C_1 p^{-(k-1)} \sum_{j=\mu}^{k} h^{j-1} \|u\|_{j, e^h}$$

$$\left(\leqslant C_1 p^{-(k-1)} \sum_{j=\mu}^{k} h^{j-1} \|\hat{u}\|_{j, (e^h)^*}\right)$$

$$\leqslant C \frac{h^{\mu-1}}{p^{k-1}} \|u\|_{k, e^h} \qquad \text{if} \quad e^h \in \mathscr{T}_0^h \tag{35}$$

$$\left(\leqslant C \frac{h^{\mu-1}}{p^{k-1}} \|\hat{u}\|_{k, (e^h)^*} \qquad \text{if} \quad e^h \in \mathscr{T}_q^h\right). \tag{36}$$

(vii) For general k we use an interpolation argument [5, 8]. The proof for the case when $\mu = k$ (i.e., $k < p+1$) is similar to the above.

(viii) (29)–(30) follow as in [9]. Q.E.D.

Suppose u_{ex} has a singularity at A_q so that $u_{\text{ex}}|_{\Omega_q} \in H^{k_q}(\Omega_q)$ and $k_q < 2$. Then, by a suitable choice of auxiliary mapping, $u_{\text{ex}} \circ \Psi_q^{-1}$ is analytic or $u_{\text{ex}} \circ \Psi_q^{-1} \in H^{k_q^*}(\Omega_q^*)$, where $k_q^* \geqslant 2$.

THEOREM 3.2. *Suppose u_p^h denotes the finite element solution of the problem (7)–(9) obtained by applying the method of auxiliary mapping with mappings Ψ_q defined in Step 2 of Section 2 in the framework of the h-p version of the finite element method over a regular family of meshes $\tilde{\mathscr{T}}$. Then*

$$\|u_{\text{ex}} - u_p^h\|_{1, \Omega} \leqslant \left[C_0 \frac{h^{\mu_0 - 1}}{p^{k_0 - 1}} \|u_{\text{ex}}\|_{k_0, \Omega_0} + \sum_{q=1}^{s} C_q \frac{h^{\mu_q - 1}}{p^{k_q^* - 1}} \|\hat{u}_{\text{ex}}\|_{k_q^*, \Omega_q^*}\right],$$

where $\mu_q = \min(p+1, k_q^*)$, $\mu_0 = \min(p+1, k_0)$, $\Omega_0 = \Omega \backslash [\bigcup_{q=1}^{s} \Omega_q]$, *and for each* $q = 0, 1, ..., s$, C_q *is a constant independent of* h *and* p.

Proof. We will proceed by modifying the proof of Theorem 4.6 of [9] and by using Lemma 3.1 and Lemma 3.2. Suppose $e_{ql}^h \in \mathscr{T}_q^h$, $e_{0m}^h \in \mathscr{T}_0^h$, $\bar{e}_{ql} \cap \bar{e}_{0m} = \gamma$, A_1 and A_2 are two endpoints of γ.

(i) If $k > \frac{3}{2}$, then by Lemma 3.2, there exist $\bar{z}_{ql} \in \mathscr{P}_p(E_1)$ and $\bar{z}_{0m} \in \mathscr{P}_p(E_2)$ (E_1 and E_2 are either T or Q) such that

$$\|u_{ex} - z_{ql}\|_{1, e_{ql}} \leqslant C_{ql} \frac{h^{\mu_q - 1}}{p^{k_q^* - 1}} \|\hat{u}_{ex}\|_{k_q^*, e_{ql}^*} \tag{37}$$

$$\|u_{ex} - z_{0m}\|_{1, e_{0m}} \leqslant C_{0m} \frac{h^{\mu_0 - 1}}{p^{k_0 - 1}} \|u_{ex}\|_{k_0, e_{0m}} \tag{38}$$

$$z_{ql}(A_j) = u_{ex}(A_j) = z_{0m}(A_j), \qquad j = 1, 2, \tag{39}$$

where $z_{ql} = \bar{z}_{ql} \circ \Phi_{e_{ql}^*}^{-1} \circ \Psi_q$ and $z_{0m} = \bar{z}_{0m} \circ \Phi_{e_{0m}}^{-1}$.

By using the techniques given in (Theorem 4.6 of [9] or Theorem 4.1 of [8]), one can modify z_{ql} and z_{0m} so that the modified functions $\tilde{z}_{ql}$ and $\tilde{z}_{0m}$ satisfy (4.9) and $\tilde{z}_{ql} = \tilde{z}_{0m}$ on γ. Repeat this correction for each side and then assemble the modified functions to obtain $\tilde{z}_p^h \in S_p^h$. Then

$$\|u_{ex} - \tilde{z}_p^h\|_{1, \Omega} \leqslant \left[C_0 \frac{h^{\mu_0 - 1}}{p^{k_0 - 1}} H^{k_0}(\Omega_0) + \sum_{q=1}^{s} C_q \frac{h^{\mu_q - 1}}{p^{k_q^* - 1}} H^{k_q^*}(\Omega_q^*) \right].$$

(ii) If $k \leqslant \frac{3}{2}$, then from the interpolation space argument as shown in Theorem 4.2 of [8] or Theorem 4.6 of [9] and case (i), we can obtain $\tilde{z}_p^h \in S_p^h$ which satisfies the required inequality. Q.E.D.

Let us note that if $f \neq 0$ then the computation of the elemental load vector is influenced by the auxiliary mapping Ψ_q. If Ψ_q is given by (15) then we have

$$\int_{\Omega_q} f \cdot v = \int_{\Omega_q^*} (m_q \omega_q)^2 r^{2(m_q \omega_q - 1)} (f \circ \Psi_q^{-1}) \hat{v}.$$

4. NUMERICAL RESULTS

In this section we make some benchmark comparisons between MAM for problems having a boundary singularity and some of the best of the alternative methods. These include finite difference, finite element, and singular function methods. The Motz problem [28, 38] and both homogeneous and nonhomogeneous Helmholtz problems are included. A variety of formats are used to present the results to facilitate later comparisons. The codes used in this benchmark study are:

- ELLPACK [32]. A second-order finite difference method over an uniform mesh in both x and y. The equations are solved by the MULTIGRID MG00 module, with a MAX of 1025 X points and 513 Y points. This method is used only on Example A. Since there is no adaptive mesh refinement, the overall convergence rate for Example A is of order one-half due to the singularity in the solution.
- PLTMG6. Bank's well-known code [11] uses a sophisticated adaptive scheme for the mesh generation using linear elements over triangles. The code has many other interesting features including a multigrid solution method. It is a research code intended to be efficient primarily in accuracy, not in time. To improve its performance the parameters ITMAX and ISPD were set to one. It easily achieves its maximum second-order accuracy over both example problems A and B.
- ISBFM. This recent code (integrated singular basis function method) is reported in [29]. It uses singular basis functions combined with biquadratic FEM basis functions over an uniform mesh. A special feature of the code is that the area integrals with singular contributions are reduced to boundary integrals by means of a double application of the divergence theorem. All results reported are reconstructed from the paper. These results show that the method quickly achieves the overall accuracy of the underlying FEM with no singularity, but at the cost of dealing with the singular functions, a set of Lagrange multipliers, and losing the original banded structure of the matrix. This method (and the related method [24, 26]) is essentially global, with the singular functions having support over all elements. Both [24, 26, 29] report severe problems with matrix conditioning for larger numbers of singular functions. No times were reported.
- FESOP. This code (finite element solution of partial differential equations), locally developed over the last nine years, uses six node isoparametric quadratic elements over triangles. The matrix is solved by an envelope method [15]. It uses an automatic mesh generation scheme based on an a priori weighting function related to known singularities. The code is highly efficient and an effort has been made to tune the power of the weighting function to these particular geometries. It easily maintains its third-order accuracy for both Examples A and B.
- MAPFEM. This code (the method of auxiliary mapping in the p-version of the finite element method), developed for elliptic problems containing singularities, is an implementation of MAM in the p-version of the finite element method as described in Section 2.2 for $1 \leqslant p \leqslant 10$. It is a research code, currently requiring hand-generated meshes. Since even the crudest mesh–with eight elements—gives better performance that the best of the others with thousands of elements, no effort has yet been made to make it efficient in time or to further increase the

p-degree. Work is underway for these features and also for an automatic mesh generation scheme. While these example problems all have only one singularity, MAPFEM is written to handle an arbitrary number of singularities, each with its own mapping region. This local nature of MAM is another of its strengths.

Another promising recent approach, the p-version of the hybrid–Trefftz method [21, 22], introduces local singular functions, while avoiding losing the original banded matrix structure by a special treatment of the interelement continuity conditions. It has the additional feature that it can handle point loads. This approach is not examined further here since it has been developed in the context of plate-bending problems and hence there is no basis for comparison in the literature for the class of problems studied in this paper.

Throughout this section, all measures of time are in seconds, and all runs have been made on a VAX/VMS 6310. For MAPFEM the absolute error in maximum norm is obtained by evaluating the absolute error at 100 points per element. We compared this approach with using 36 points per element and found only small differences. We also evaluated the error along two radial lines at angles 0° and 45° from the positive x-axis and found, as expected, no large errors near the origin. In Examples A and B for the computation of the maximum error we used known approximations or solutions. In Example C no known results are available for comparison. To determine the relative error in the energy norm in Examples A, B, and C we use the method in Chapter 4 of [36] which estimates the true total energy by extrapolation using the three best computed total energies. "with mapping" stands for the case when MAM is applied and "without mapping" stands for the case when MAM is *not* applied. ASM stands for the CPU time for assembling the local stiffness matrices and load vectors and SOL stands for the CPU time for factoring and solving the algebraic system. According to Corollary 2.1, the column (with mapping) should be the same as the column (without mapping) in Table A.IV. However, our research computer code, which is designed to cover general elliptic operators, made unnecessary computations for the coefficients q_{11} and q_{22} of Theorem 2.1, adding slightly to the time.

Our first benchmark is a classic Laplace equation problem with a singular solution, known in the literature [24–26, 28, 29, 33, 37, 38, 40] as the Motz problem. Examples in this section have essential boundary conditions. For standard arguments to deal with essential boundary conditions in finite element approximations, we refer to [8, 14, 36]. From arguments in [3, 4, 20] with suitable regularity requirements on the boundary data, Theorem 3.1 is valid for elliptic problems with essential boundary conditions on parts of the boundary away from the singular regions.

EXAMPLE A (The Motz Problem). Let Ω and Γ_i be the domain and edges depicted in Fig. 4.1. Let us consider the problem (7)–(9) with the following data:

$$-\Delta u = 0 \qquad \text{on } \Omega,$$

$$u = \begin{cases} 500 & \text{on } \Gamma_2 \\ 0 & \text{on } \Gamma_6 \end{cases}$$

$$\frac{\partial u}{\partial n} = 0 \qquad \text{on } \Gamma_1 \cup \Gamma_3 \cup \Gamma_4 \cup \Gamma_5.$$

For MAM we use an eight element mesh and two refinements with 32 and 48 elements respectively. It should be noted that the last refinement was chosen away from the singularity. In Fig. 4.1, $(r, 0) = (0.8, 0)$ when MAM is used and $(r, 0) = (0.5, 0)$ when MAM is not used. In Mesh II and Mesh III (Fig. 4.2), the radii of the semicircles are 0.8, 0.6, 0.3, respectively, when MAM is applied. On the other hand, the radii are 0.8, $0.8 \times (0.15)$, $0.8 \times (0.15)^2$, respectively, when MAM is not used. It is well known that such geometric mesh refinement leads to optimal results. These meshes are used for values of p, $1 \leqslant p \leqslant 10$. For ELLPACK an uniform mesh of size $(N+1)$ by $(2N+1)$ with $2^3 \leqslant N \leqslant 2^9$ is used (no figure). PLTMG6 is used with 56 to 6390 nodes with the case of 3198 nodes illustrated in Fig. 4.3. FESOP is used with 73 to 15,303 nodes with the case of 5167 nodes and 2500 elements illustrated in Fig. 4.4. ISBFM is reported [29] over uniform meshes of size N by $2N$ with $N = 1, 2, 4$, and 8 using biquadratic basis elements, using two singular functions and an appropriate number of Lagrange multipliers (no figure).

For comparison with other methods, ELLPACK, PLTMG6, ISBFM, and FESOP are applied to the Motz problem. In [24, 26] an effort is made to give an extremely accurate solution to the Motz problem for use as benchmarks such as in this study. Solutions of the form

$$u = \sum_{l=0}^{34} b_l r^{l+1/2} \cos\left(l + \tfrac{1}{2}\right)\theta \tag{40}$$

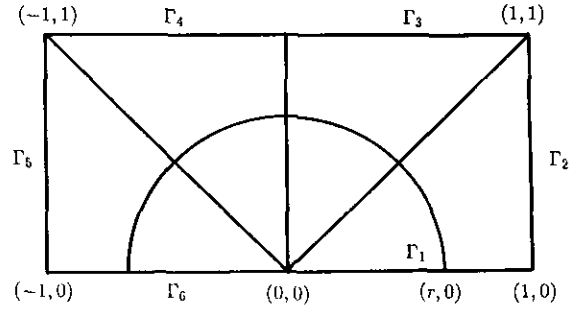

FIG. 4.1. The domain Ω, a singular neighborhood $\Omega_{(0,0)}$, and Mesh I for MAPFEM.

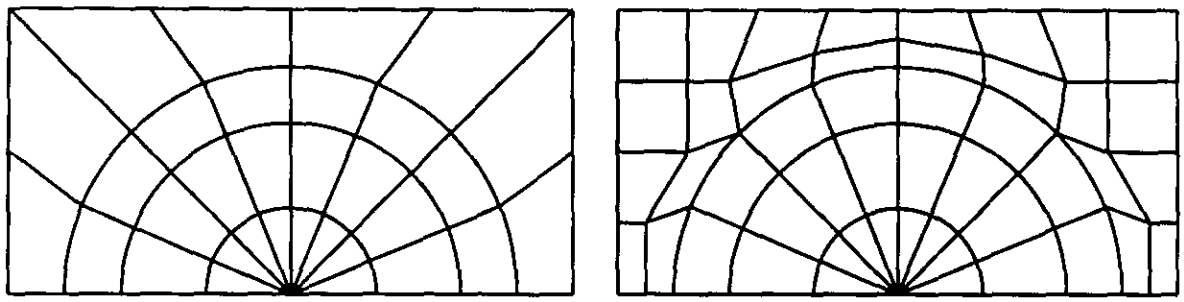

FIG. 4.2. Mesh II for MAPFEM (32 elements) and Mesh III for MAPFEM (48 elements).

are found by requiring the boundary conditions along $x = -1$, $x = 1$, and $y = 1$ to be satisfied in the sense of least squares. It is claimed that the maximum error on $x = 1$ is 5.47E-09. When attempting to replicate these results using the values for b_i found in [24, 26] along $(1, y)$ for $0 \leqslant y \leqslant 1$ we found an error of over 1.5E-04 when compared with the true value of $u = 500$ along $x = 1$. Further study lead to the discovery that the error had a pattern which suggested that the coefficient b_{31} was in error. Dividing b_{31} by 10 improved the results to an error of only 5.48E-09 along $x = 1$ as originally claimed. While the actual accuracy of these results is apparently not known, the claim made in [26] that they are "The most accurate solution of the Motz problem ever published (1987)" seems well justified. However, it should be noted that Rosser and Papamichael in 1975 [33] succeeded in finding a *closed form* solution to the Motz problem, using a succession of six conformal mappings. In order to express this solution in a form suitable for computations they reduced their expressions to the form (40) but with 20 terms instead of 35 and numbers of significant digits decreasing from 20 for b_0 to 4 for b_{19}. Thus their solution is the most accurate known for small r, but is less accurate than (40) by several significant digits near the far corners. Equation (40) with a recursion relationship for the next cosine term, is easy to apply and is used as the true solution for all maximum norm comparisons with the Motz problem.

The results obtained by ELLPACK, PLTMG6, and FESOP are listed in Table A.I. For convenience over so many codes, the comparison results are all computed in the maximum norm. The convergence is of order $\frac{1}{2}$, 2, and 3 for these methods, respectively. The ELLPACK run, with over a half million nodes in 10 s, shows the futility of brute force techniques. The results for MAPFEM with Meshes I, II, and III are given in Table A.II for both the absolute error in the maximum norm and the relative error in the energy norm. As was noted in Section 2.1, the energy norm is equivalent to the H^1 norm used in Theorems 3.1 and 3.2. In Table A.III the ordinary p method (without use of MAM is applied over a geometric mesh refinement topologically equivalent to Meshes I, II, and III as detailed above. The results are inferior as expected. Also in Table A.III, the degrees of freedom (which are the same with or without MAM) are given, and in Table A.IV the CPU times are

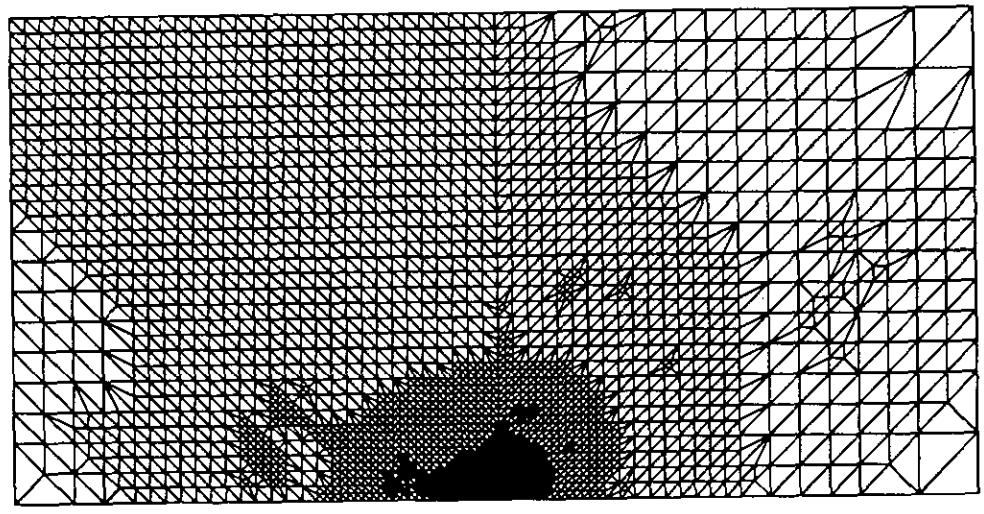

FIG. 4.3. Adaptive mesh for PLTMG6 with 3198 nodes for Example A (it is similar for Example B).

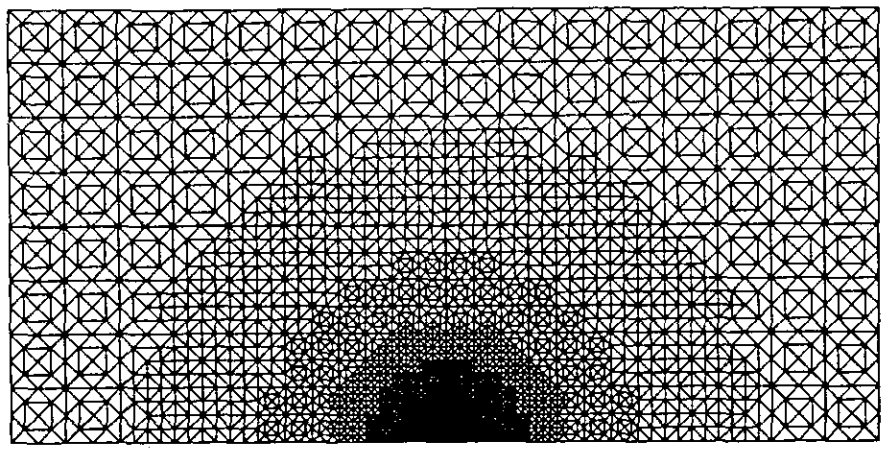

FIG. 4.4. Adaptive mesh for FESOP with 2500 elements and 5167 nodes for Examples A and B.

given. In Fig. 4.5 an overall comparison of the absolute error in the maximum norm versus the degrees of freedom is made between the results of ELLPACK, PLTMG6, FESOP, and the MAM code MAPFEM using Meshes I, II, and III. The exponential convergence of Theorem 3.1 for the energy norm is observed even in this case and the improvements generated by the *h-p* method of Theorem 3.2 can be seen by comparing the MAM results over the three meshes. Our best result, MAM with Mesh III and $p = 10$, shows a relative improvement of over 10 orders of magnitude. Its error of 2.22E–08 is determined by comparison with (40) which has a known lower error bound of 5.48E–09. Here it is not obvious which approximate solution (MAPFEM or (40)) is better. The $p = 10$ case with Mesh III appears to be losing exponential convergence. This could be explained by the above or an alternative possibility is that an insufficient number of Gauss points (12 by 12 grid) were used for the required high order numerical integrations when $p = 12$. Selected computational times are included in Fig. 4.5 for all of the above methods. In Fig. 4.6 we compare the relative energy error versus the square root of the number of degrees of freedom of MAPFEM over the three meshes with the singular basis code ISBFM [29] using two singular functions. The convergence of the three MAPFEM results is clearly exponential, while the ISBFM code is limited by the convergence rate of the underlying

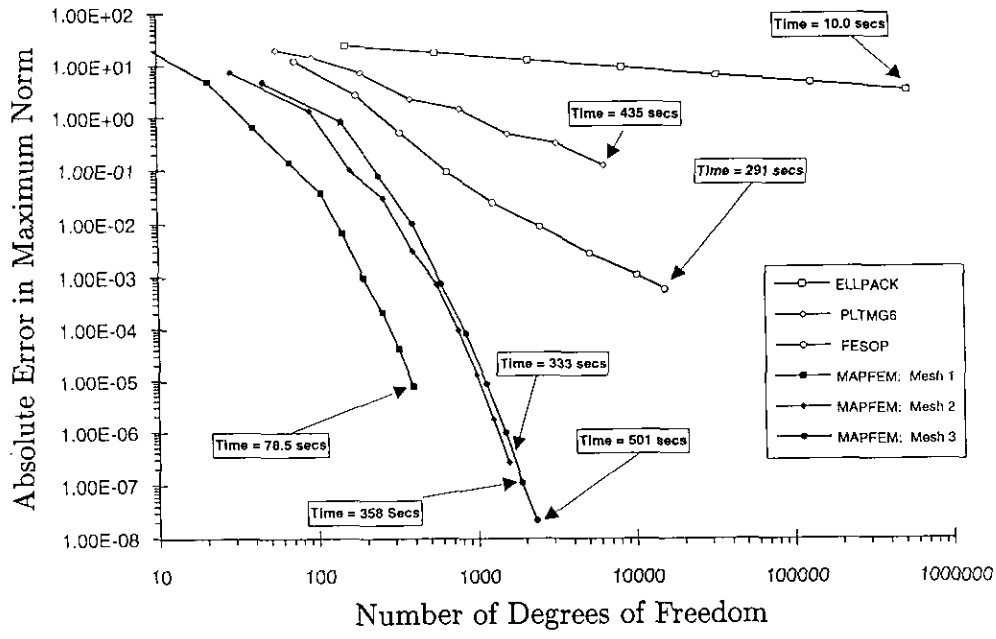

FIG. 4.5. Overall comparisons for the Motz problem in maximum norm.

TABLE A.I

Number of Nodes, CPU Time, and Maximum Errors for PLTMG6, ELLPACK, and FESOP Applied to the Motz Problem

ELLPACK			PLTMG6			FESOP		
Nodes	Time	Max. error	Nodes	Time	Max. error	Nodes	Time	Max. error
153	0.01	25.90	56	1.46	20.92	73	0.58	1.29D+01
561	0.01	19.00	94	2.63	15.18	179	1.01	2.79D−00
2,145	0.02	13.70	191	5.88	7.62	335	1.52	5.44D−01
8,385	0.10	9.83	392	18.38	2.36	657	2.50	9.74D−02
33,153	0.38	7.00	799	32.07	1.50	1,277	5.29	2.60D−02
131,841	1.53	4.97	1591	85.66	0.51	2,523	12.55	9.20D−03
525,825	10.02	3.52	3198	160.27	0.34	5,167	44.39	2.95D−03
			6390	434.98	0.13	10,259	141.52	1.10D−03
						15,303	291.43	6.12D−04

TABLE A.II

The Absolute Error in Maximum Norm and the Relative Error in Energy Norm for MAM

	Abs. error in max. norm			Rel. error in energy norm		
p	Mesh I	Mesh II	Mesh III	Mesh I	Mesh II	Mesh III
1	4.11D+01	7.77D−00	4.77D−00	2.33D−01	9.25D−02	7.19D−02
2	4.98D+00	1.38D−00	8.62D−01	5.02D−02	1.39D−02	9.00D−03
3	6.62D−01	1.05D−01	8.10D−02	1.05D−02	2.19D−03	1.74D−03
4	1.44D−01	3.09D−02	1.05D−02	2.70D−03	5.15D−04	2.38D−04
5	3.80D−02	3.25D−03	7.56D−04	6.39D−04	8.91D−05	2.97D−05
6	6.76D−03	7.50D−04	8.42D−05	1.39D−04	1.45D−05	3.42D−06
7	9.87D−04	9.45D−05	8.83D−06	3.23D−05	2.57D−06	4.16D−07
8	2.16D−04	1.34D−05	1.00D−06	7.37D−06	4.62D−07	4.83D−08
9	4.35D−05	1.85D−06	1.11D−07	1.72D−06	—	—
10	8.02D−06	2.67D−07	2.22D−08	3.70D−07	—	—

TABLE A.III

The Number of Degrees of Freedom and the Relative Error in the Energy Norm When MAM Is *Not* Applied

	Degrees of freedom			Rel. error in energy norm		
p	Mesh I	Mesh II	Mesh III	Mesh I	Mesh II	Mesh III
1	6	29	47	3.22D−01	2.70D−01	1.65D−01
2	21	91	143	1.74D−01	1.55D−01	5.51D−02
3	40	161	247	1.25D−01	1.11D−01	2.88D−02
4	67	263	399	9.73D−02	8.60D−02	1.93D−02
5	107	397	599	7.98D−02	7.04D−02	1.51D−02
6	145	563	847	6.76D−02	5.96D−02	1.28D−02
7	196	761	1143	5.87D−02	5.17D−02	1.10D−02
8	255	991	1487	5.18D−02	4.56D−02	9.67D−03
9	322	1253	1879	4.64D−02	4.08D−02	8.65D−03
10	397	1547	2319	4.20D−02	3.69D−02	7.83D−03

TABLE A.IV

The CPU Time for the Motz Problem

		With mapping			Without mapping		
	p	Mesh I	Mesh II	Mesh III	Mesh I	Mesh II	Mesh III
ASM	3	4.00	14.79	18.38	3.64	12.38	17.50
SOL	3	0.82	2.99	4.69	0.82	2.99	4.69
ASM	5	8.50	32.91	45.68	8.17	31.74	45.10
SOL	5	2.43	10.87	17.13	2.43	10.87	17.13
ASM	8	28.30	111.29	161.65	28.06	107.69	159.20
SOL	8	10.36	49.63	81.44	10.36	49.63	81.44
ASM	9	40.65	158.36	237.06	40.22	156.52	234.56
SOL	9	20.37	75.90	121.03	20.37	75.90	121.03
ASM	10	56.65	222.61	325.51	56.60	220.15	321.80
SOL	10	21.90	110.05	175.50	21.90	110.05	175.50

Note. ASM stands for the CPU time for assembling the local stiffness matrices and load vectors and SOL stands for the CPU time for factoring and solving the algebraic system.

FEM basis functions just as in the case of PLTMG6 and FESOP. There was uncertainty in the calculation of the energy errors (using the extrapolation method) for $p > 8$ with MAPFEM on Meshes II and III so these are not reported. In Fig. 4.7 we compare absolute accuracy in the maximum norm versus time for ELLPACK, PLTMG6, FESOP, and MAPFEM for the Motz problem. The curve in the FESOP results is explained by a conversion from time dominance of the matrix assembly to the more costly matrix solution as n increases. While the three MAPFEM results again clearly stand out and are impressive, the time results given are nevertheless limited by the current state of the MAPFEM code. We anticipate improvement here as MAPFEM matures.

In the next two examples we consider Helmholtz equations containing singularities: Example B and Example C are about homogeneous and nonhomogeneous Helmholtz equations, respectively. In Examples B and C, Ω and Γ_i are the same as those depicted in Fig. 4.1. Mesh I, Mesh II, and Mesh III on Ω are given in Fig. 4.1 and Fig. 4.2.

EXAMPLE B. Let us consider a homogeneous Helmholtz equation containing a singularity:

$$-\Delta u + u = 0 \qquad \text{on } \Omega,$$

$$u = \begin{cases} \dfrac{\sinh(r)}{\sqrt{r}}\cos(\theta/2) & \text{on } \partial\Omega - \Gamma_1 - \Gamma_6 \\ 0 & \text{on } \Gamma_6 \end{cases}$$

$$\frac{\partial u}{\partial n} = 0 \qquad \text{on } \Gamma_1.$$

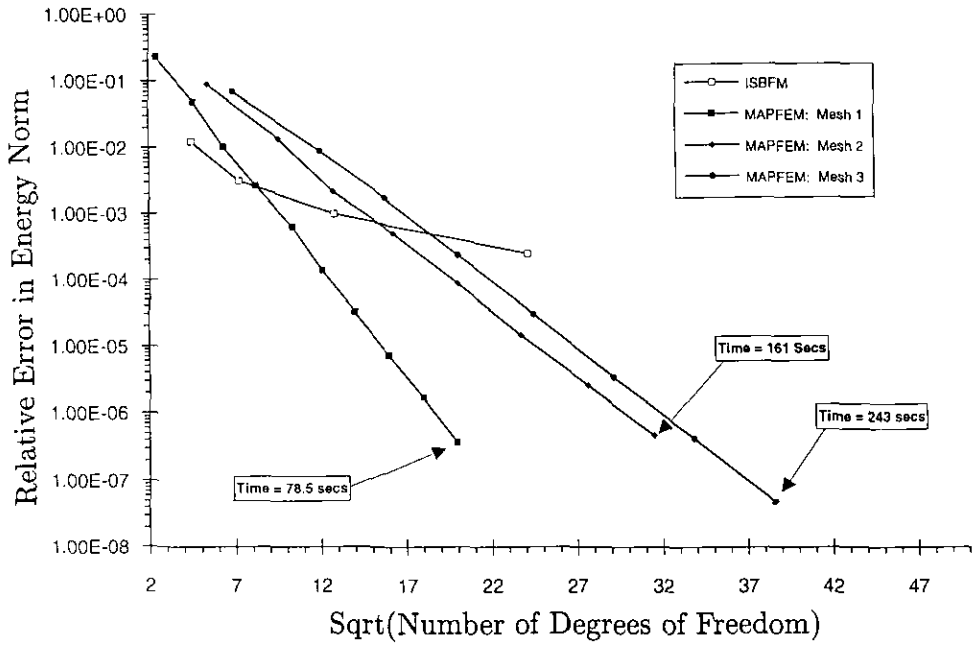

FIG. 4.6. Relative errors of finite element solutions for the Motz problem in energy norm.

Then this problem has a strong boundary singularity at (0, 0) and the true solution is

$$u(r, \theta) = \frac{\sinh(r)}{\sqrt{r}} \cos(\theta/2). \tag{41}$$

The absolute error in the maximum norm, number of nodes, and CPU time for PLTMG6 and FESOP are given in Table B.I. The p degree, degrees of freedom, and absolute error for MAPFEM for Meshes I and III are given in Table B.II. These results for the homogeneous Helmholtz problem, after adjusting by the factor of 500, are similar to the previous ones, so they are presented in less detail. The results are summarized in Fig. 4.8 which shows that the convergence is exponential for MAPFEM, but algebraic for PLTMG6 and FESOP. MAPFEM with eight elements and

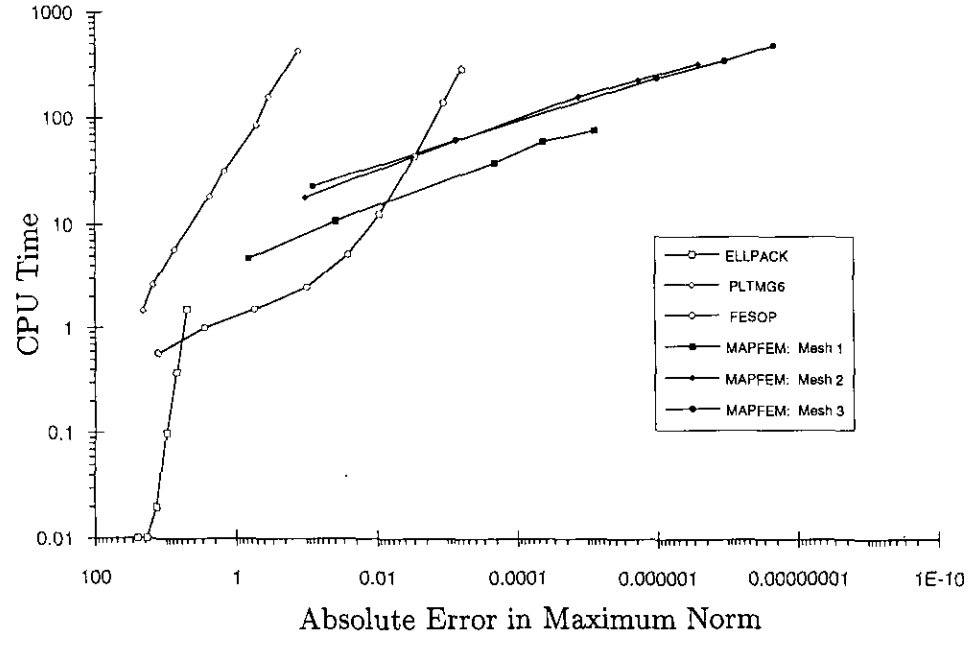

FIG. 4.7. *Accuracy versus time comparison for the Motz problem.*

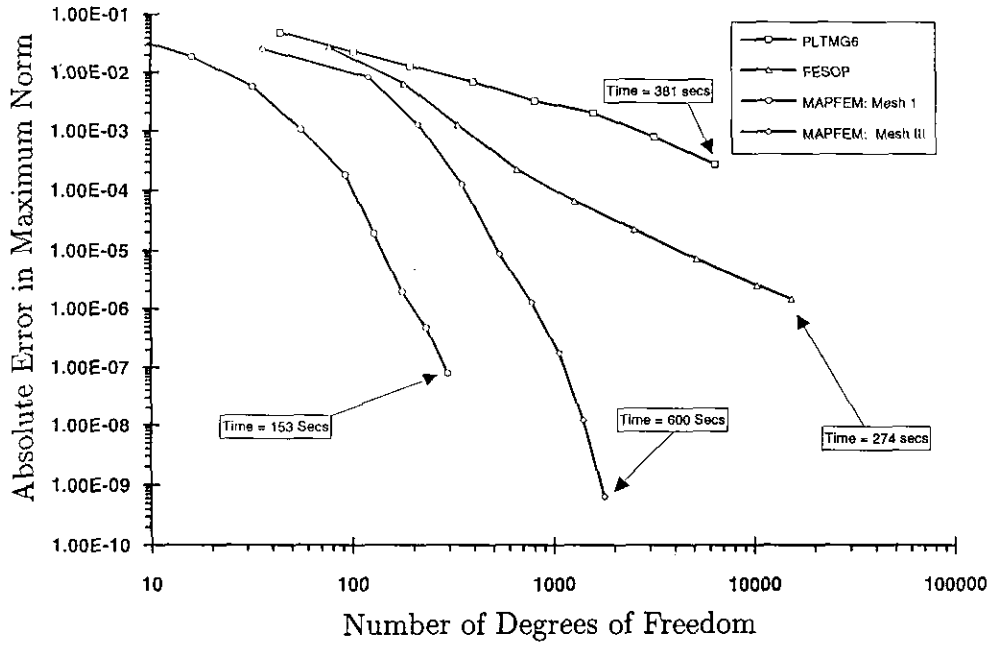

FIG. 4.8. Comparing solution methods for the homogeneous Helmholtz equation in maximum norm.

TABLE B.I

Nodes, CPU Time, and Maximum Errors for PLTMG6 and FESOP

PLTMG6			FESOP		
Nodes	Time	Max. error	Nodes	Time	Max. error
44	1.16	5.13D−02	77	0.66	2.94D−02
102	2.87	2.43D−02	179	1.03	6.95D−03
195	6.90	1.38D−02	335	1.56	1.36D−03
398	13.28	7.43D−03	657	2.81	2.41D−04
810	29.58	3.47D−03	1,277	5.67	7.04D−05
1,590	65.82	2.19D−03	2,523	13.48	2.38D−05
3,191	140.45	8.56D−04	5,167	40.38	7.52D−06
6,395	381.45	2.98D−04	10,259	129.13	2.70D−06
			15,303	273.8	1.56D−06

TABLE B.II

Maximum Errors for MAPFEM on Mesh I and Mesh III

	MAPFEM			
p-degree	Mesh I	DOF	Mesh III	DOF
1	8.11D−02	4	2.67D−02	36
2	1.93D−02	16	8.74D−03	120
3	5.95D−03	32	1.35D−03	212
4	1.10D−03	56	1.34D−04	352
5	1.89D−04	93	8.99D−06	540
6	1.97D−05	128	1.33D−06	776
7	2.01D−06	176	1.86D−07	1060
8	4.77D−07	232	1.27D−08	1392
9	8.25D−08	296	6.48D−10	1772

296 degrees of freedom is better than the best of the comparison methods (FESOP) with 15,303 nodes by a factor of 19 while taking just over half the time. There are over two orders of magnitude improvement achieved by going to Mesh III. The CPU times of MAPFEM for this problem on Mesh I and Mesh III are 152.97 s and 599.66 s, respectively.

EXAMPLE C. Let us consider a *nonhomogeneous* Helmholtz equation containing a singularity:

$$-\Delta u + u = 1 \qquad \text{on } \Omega,$$

$$u = \begin{cases} 500 & \text{on } \Gamma_2 \\ 0 & \text{on } \Gamma_6 \end{cases}$$

$$\frac{\partial u}{\partial n} = 0 \qquad \text{on } \Gamma_1 \cup \Gamma_3 \cup \Gamma_4 \cup \Gamma_5.$$

The relative errors in energy norm are listed in Table C.I. In Table C.I., Mesh I, Mesh II, and Mesh III give the results obtained by the p-version of the finite element method with MAM on their respective meshes while Meshes 1, 2, and 3 refer to the p-version without mapping. No comparison runs are made for this example since the solution is unknown. The relative errors in energy versus the square root of the degrees of freedom (as given in Table A.III) are plotted in Fig. 4.9 for MAM over Meshes I, II, and III and without mapping over Mesh 3. As was shown in [6], if $f \neq 0$, MAM can not completely remove the singularity effect caused by irregular geometry or changes of boundary data. However, in this particular problem, the interior angle $\pi\omega$ at (0, 0) is π and hence $(k + 1/2)/\omega$ cannot be an integer

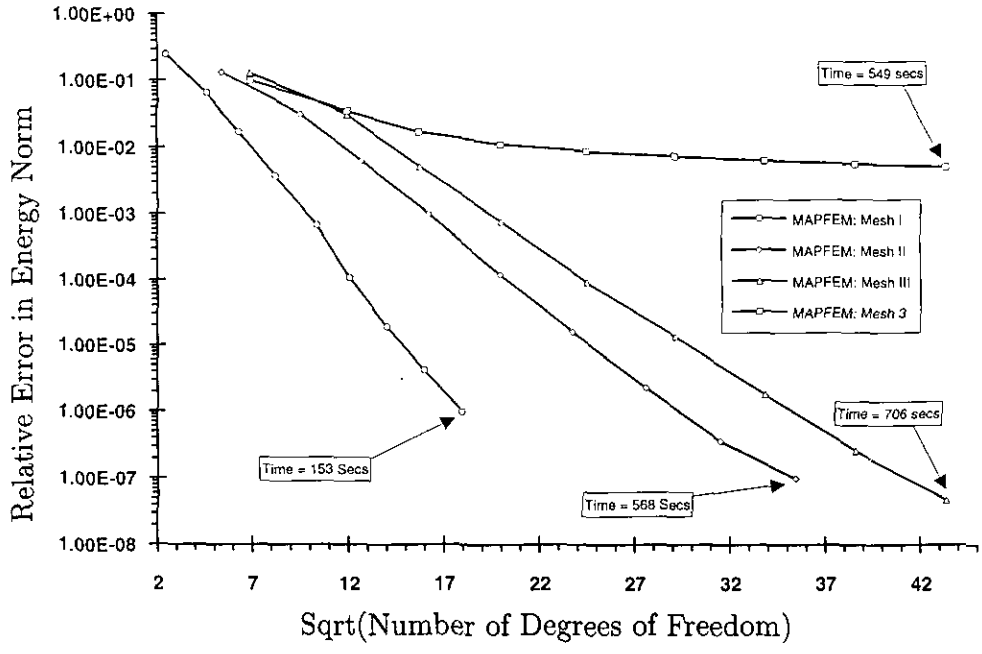

FIG. 4.9. Relative errors of finite element solutions for the nonhomogeneous Helmholtz equation in energy norm.

TABLE C.I

The Relative Error in Energy Norm for the Nonhomogeneous Helmholtz Equation

	With mapping			Without mapping		
	Mesh I	Mesh II	Mesh III	Mesh I	Mesh II	Mesh III
1	2.51D−01	1.36D−01	1.31D−01	2.16D−01	1.09D−01	1.01D−01
2	6.52D−02	3.16D−02	3.12D−02	1.05D−01	3.54D−02	3.50D−02
3	1.75D−02	6.46D−03	5.28D−03	7.42D−02	1.78D−02	1.73D−02
4	3.77D−03	1.01D−03	7.85D−04	5.65D−02	1.12D−02	1.12D−02
5	6.87D−04	1.22D−04	9.16D−05	4.62D−02	8.75D−03	8.75D−03
6	1.10D−04	1.59D−05	1.34D−05	3.91D−02	7.33D−03	7.33D−03
7	1.92D−05	2.27D−06	1.80D−06	3.40D−02	6.34D−03	6.34D−03
8	4.21D−06	3.56D−07	2.57D−07	3.00D−02	5.59D−03	5.59D−03
9	9.86D−07	1.00D−07	4.73D−08	2.69D−02	5.00D−03	5.00D−03

TABLE C.II

The CPU Time for $-\Delta u + u = 1$ on $\Omega = [-1, 1] \times [0, 1]$

		With mapping			Without mapping		
	p	Mesh I	Mesh II	Mesh III	Mesh I	Mesh II	Mesh III
ASM	5	31.06	139.60	172.45	19.66	116.26	147.63
ASM	8	106.55	406.36	507.63	55.66	302.85	403.03
ASM	9	153.00	568.34	706.61	79.53	414.43	548.60

for any integer k. Thus, no terms in the asymptotic expansion of u_{ex} contain $\log r$ (see, [17]). Therefore, MAM can transform the singular solution $u_{ex}|_{\Omega_{(0,0)}}$ to an analytic function on $\hat{u}|_{\Omega^*_{(0,0)}}$. Thus, MAM gives rise to exponential convergence as one can observe from Fig. 4.9.

If $\varphi: \Omega^* \to \Omega$ is an auxiliary mapping, then

$$\iint_{\Omega} uv \, d\Omega = \iint_{\Omega^*} |J(\varphi)| \hat{u}\hat{v} \, d\Omega^*.$$

Because of the additional computation of the Jacobian $|J(\varphi)|$ in the above equation, for Helmholtz equations, the CPU time when MAM is used is larger than that when MAM is not used. One can see the difference in Table C.II. Of course, SOL for this example is the same as those in Table A.III.

5. CONCLUDING REMARKS

The method of auxiliary mapping has been shown to converge exponentially for the Laplace and Helmholtz equations with several corner and boundary singularities. An additional convergence result has been obtained for the h-p version of the finite element method. Benchmark studies have been made comparing MAM with the finite difference code ELLPACK, the adaptive fintie element codes PLTMG6 and FESOP both in accuracy and time, and the singular element code ISBFM in accuracy. For the Motz problem (Example A) even our simplest mesh with eight

elements gives an absolute error in the maximum norm of almost eight orders of magnitude improvement (from 500 to 8.0E–06) in 79 s, while denser meshes give over two additional orders of improvement. The latter result (2.0E–08) is at least very close to the most accurate solution known to the Motz problem [24, 26]. Finally the method, as we have implemented it, is straightforward to apply to new problems and has an essentially local nature. While it is currently fast for a given accuracy compared to other methods, no effort so far has been made to optimize it. As mapping methods for singular problems grow more popular we anticipate the development of optimized mapping codes that will further increase the competitive advantage of this family of methods.

ACKNOWLEDGMENTS

The authors thank Professor Nick Papamichael for drawing their attention to Refs. [18, 33] and to one of the referees for suggesting that Ref. [22] should be mentioned.

REFERENCES

1. I. E. Akin, *Int. J. Numer. Methods Eng.* **10**, 1249 (1976).
2. I. Babuška and B. Guo, *SIAM J. Numer. Anal.* **25**, 837 (1988).
3. I. Babuška and B. Guo, *Comput. Methods Appl. Mech. Eng.* **74**, 1 (1989).
4. I. Babuška and B. Guo, *SIAM J. Math. Anal.* **19**, 172 (1988).
5. I. Babuška, B. Kellogg, and J. Pitkäranta, *Numer. Math.* **33**, 447 (1979).
6. I. Babuška and H.-S. Oh, *Numer. Methods Partial Differential Eqs.* **6**, 371 (1990).
7. I. Babuška and M. R. Rozenzweig, *Numer. Math.* **20**, 1 (1972).
8. I. Babuška and M. Suri, *SIAM J. Numer. Anal.* **24** (4), 750 (1987).
9. I. Babuška and M. Suri, *Math. Modelling Numer. Anal.* **21**, 199 (1987).
10. I. Babuška, B. A. Szabo, and I. N. Katz, *SIAM J. Numer. Anal.* **18**, 515 (1981).
11. R. E. Bank, *PLTMG6: A Software Package for Solving Elliptic Partial Differential Equations User's Guide 6.0* (SIAM, Philadelphia, 1990).
12. P. G. Ciarlet, *The Finite Element Method for Elliptic Problems* (North-Holland, Amsterdam, 1978).
13. G. Fix, S. Gulati, and G. I. Wakoff, *J. Comput. Phys.* **13**, 209 (1973).
14. G. Fix, M. Gunzburger, and J. Peterson, *Comput. Math. Appl.* **9**, 687 (1983).
15. A. George and J. W.-H. Liu, *Computer Solutions of Large Sparse Positive Definite Systems* (Prentice-Hall, Englewood Cliffs, NJ, 1981).
16. W. Gordon and C. Hall, *Int. J. Numer. Methods Eng.* **7**, 461 (1973).
17. P. Grisvard, *Elliptic Problems in Nonsmooth Domains* (Pitman, New York, 1985).
18. P. Grisvard, W. Wendland, and J. R. Whiteman, *Singularities and Constructive Methods for Their Treatment*, Lecture Notes in Math., Vol. 1121 (Springer-Verlag, New York/Berlin, 1983).
19. B. Guo and I. Babuška, *The h-p Version of the Finite Element Method. Part 1. The Basic Application Results* **1**, 21 (1986).
20. B. Guo and I. Babuška, *The h-p Version of the Finite Element Method. Part 2. General Results and Applications* **1**, 203 (1986).
21. J. Jirousek, *Int. J. Numer. Methods Eng.* **24**, 1367 (1987).
22. J. Jirousek and A. Venkatesh, *Comput. & Structures* **37**, 217 (1990).
23. V. A. Kondrat'ev, *Trans. Moscow Math. Soc.* **16**, 227 (1967).
24. Z.-C. Li Dissertation, University of Toronto, 1986 (unpublished).
25. Z. C. Li, *Numer. Math.* **49**, 475 (1986).
26. Z. C. Li, R. Mathon, and P. Sermer, *SIAM J. Numer. Anal.* **24**, 487 (1987).
27. V. P. Mikhailov, *Partial Differential Equations* (MIR, Mosow, 1978).
28. H. Motz, *Q. Appl. Math.* **4**, 371 (1946).
29. L. G. Olson, G. C. Georgiou, and W. W. Schultz, *J. Comput. Phys.* **96**, 391 (1991).
30. H.-S. Oh, "The *p*-Version of the Finite Element Method for Three-Dimensional Elliptic Problems Containing Vertex and Edge Singularities," in *Proceedings in Honor of Professor C. N. Lee on his Sixtieth Birthday* (Dept. of Math. Postech, Pohang, Korea, 1991).
31. H.-S. Oh and I. Babuška, *Comput. Methods Appl. Mech. Eng.*, to appear.
32. J. R. Rice and R. F. Boisvert, *Solving Elliptic Problems using ELLPACK* (Springer-Verlag, New York/Berlin, 1985).
33. J. B. Rosser and N. Papamichael, MRC Technical Summary Report No. 1405, University of Wisconsin, 1975 (unpublished).
34. M. Stern, *Int. J. Numer. Methods Eng.* **14**, 409 (1979).
35. G. Strang and G. Fix, *An Analysis of the Finite Element Method* (Prentice-Hall, Englewood Cliffs, NJ, 1973).
36. B. A. Szabo and I. Babuška, *Finite Element Analysis* (Wiley, New York, 1990).
37. R. W. Thatcher, *Numer. Math.* **25**, 163 (1976).
38. R. Wait and A. R. Mitchell, *J. Comput. Phys.* **8**, 45 (1971).
39. J. R. Whiteman, N. Papamichael, and Q. Martin, "Conformal Transformation Methods for the Numerical Solution of Harmonic Mixed Boundary Value Problems," Conference on Applications of Numerical Analysis, Lecture Notes in Math. Vol. 228 (Springer-Verlag, New York/Berlin, 1971).
40. J. R. Whiteman and N. Papamichael, *Aqnew. Math. Phys.* **23**, 655 (1972).
41. M. Zlamal, *SIAM J. Numer. Anal.* **10**, 229 (1973).